Technical note: Measurement of chemically-resolved volume equivalent diameter and effective density of particles by AAC-SPAMS

Long Peng[1,2], Lei Li[4], Guohua Zhang[1, 3*], Xubing Du[4], Xinming Wang[1, 3], Ping'an Peng[1, 3], Guoying Sheng[1], Xinhui Bi[1, 3*]

[1] State Key Laboratory of Organic Geochemistry and Guangdong Provincial Key Laboratory of Environmental Protection and Resources Utilization, Guangzhou Institute of Geochemistry, Chinese Academy of Sciences, Guangzhou 510640, China

[2] University of Chinese Academy of Sciences, Beijing, 100049, China

[3] Guangdong-Hong Kong-Macao Joint Laboratory for Environmental Pollution and Control, Guangzhou 510640, China

[4] Institute of Mass Spectrometer and Atmospheric Environment, Jinan University, Guangzhou 510632, China

*Correspondence to: bixh@gig.ac.cn and zhanggh@gig.ac.cn

Abstract

Size and effective density (ρ_e) are important properties of aerosol particles and are related to their influences on human health and the global climate. The volume equivalent diameter (D_{ve}) is an intrinsic property that is used to evaluate particle size. ρ_e, defined as the ratio of particle density to a dynamic shape factor (χ), is used to characterize the physical property of a particle as an alternative to particle density. However, it is still challenging to simultaneously characterize the D_{ve} and ρ_e of particles. Here, we present a novel system that classifying particles with their aerodynamic diameter (D_a) by aerodynamic aerosol classifiers (AAC) and determining their vacuum aerodynamic diameter (D_{va}) by single particle aerosol mass spectrometry (SPAMS) to achieve a measurement of D_{ve} and ρ_e. The reliability of the AAC-SPAMS system for accurately obtaining D_{ve} and ρ_e is verified based on the results that the deviation between the measured values and the theoretical values is less than 6% for the size-resolved spherical polystyrene latex (PSL). The AAC-SPAMS system is applied to characterize the D_{ve} and ρ_e of $(NH_4)_2SO_4$ and $NaNO_3$ particles, suggesting that these particles are aspherical and their ρ_e are independent of particle size. Finally, the AAC-SPAMS system is deployed in a field measurement, showing that it is a powerful technique to characterize the chemically-resolved D_{ve} and ρ_e of particles in real time.

1. Introduction

Size and particle density (ρ_p) are critical parameters of aerosol particles in quantifying the impact of aerosols on air quality, human health and global climate change (Buseck and Posfai, 1999; Poschl, 2005; Pitz et al., 2003). Effective density (ρ_e) has been adopted to characterize the physical property of a particle as an alternative to ρ_p, since ρ_p for aspherical aerosol particles is hardly measured (Sumlin et al., 2018; Katrib et al., 2005). Size and ρ_e govern the transport properties of a particle both in the atmosphere and in the human respiratory system (Seinfeld and Pandis, 1998; Liu and Daum, 2008) and directly/indirectly influence the potential of the particle to absorb or reflect solar radiation (Tang, 1997; Zhao et al., 2019; Liu and Daum, 2008). ρ_e can also provide information concerning particle morphology (Yon et al., 2015) and serve as a tracer for atmospheric processing (Guo et al., 2014; Yin et al., 2015; Liu et al., 2015). However, the quantitative relationship between aerosol properties, namely, size and ρ_e, and their effects on air quality, human health and global climate change is not yet well understood, which is partly because important aerosol properties cannot be measured by current techniques.

Size. Size is a fundamental property of particles, which can be parameterized by the physical quantity of volume equivalent diameter (D_{ve}). Defined as the diameter of a spherical particle with the same volume as the particle (DeCarlo et al., 2004), D_{ve} is an intrinsic physical quantity that can be used to evaluate the actual size of the particle. However, to date, atmospheric science usually describes particle size by other diameter definitions, such as the electric mobility diameter (D_m), aerodynamic equivalent

diameter (D_a) and vacuum aerodynamic equivalent diameter (D_{va}), whose relationships with D_{ve} are shown in Eqs. (1)-(3), respectively:

$$\frac{D_m}{C_c(D_m)} = \frac{D_{ve}}{C_c(D_{ve})}\chi_t, \quad (1)$$

$$D_a = D_{ve}\sqrt{\frac{\rho_p C_c(D_{ve})}{\chi_t \cdot \rho_0 \cdot C_c(D_a)}}, \quad (2)$$

$$D_{va} = \frac{\rho_p}{\rho_0}\frac{D_{ve}}{\chi_v}, \quad (3)$$

where $C_c(D)$ is the Cunningham slip correction factor, χ_t and χ_v represent the aerosol dynamic shape factor (χ) in the transition regime and in the free-molecule regime, respectively, and ρ_0 represents the unit density of 1.0 g/cm^3. From the definitions, it can be seen that D_m, D_a, and D_{va} are originally derived from D_{ve}, but in actuality, they do not reflect the actual size of the particle. Meanwhile, D_{ve} cannot be easily obtained, which limits its application in the scientific community.

Effective density. At present, three definitions of ρ_e are introduced in atmospheric science (DeCarlo et al., 2004): the first definition (ρ_e^I) is the ratio of the measured particle mass (m_p) to the particle volume (V) calculated assuming a spherical particle with a diameter equal to the measured D_m; the second definition (ρ_e^{II}) is the ratio of ρ to χ (Hand and Kreidenweis, 2002); and the third definition (ρ_e^{III}) is the ratio of D_m and D_{va}, all of which are expressed in Eqs. (4)-(6), respectively.

$$\rho_e^I = \frac{6m_p}{\pi {D_m}^3} \quad (4)$$

$$\rho_e^{II} = \frac{\rho_p}{\chi} \quad (5)$$

$$\rho_e^{III} = \frac{D_{va}}{D_m}\rho_0 \quad (6)$$

The definitions of ρ_e^I and ρ_e^{III} can be derived into the final forms, as shown in the Eqs.(7) and (8), respectively.

$$\rho_e^{\mathrm{I}} = \frac{\rho}{\chi_t^3} \cdot \left(\frac{C_c(D_{ve})}{C_c(D_m)}\right)^3 \quad (7)$$

$$\rho_e^{III} = \rho \cdot \frac{C_c(D_{ve})}{\chi^2 \cdot C_c(D_m)} \quad (8)$$

The Eq. (7) is derived from combining the Eq. (1) with Eq. (4) in which m_p is equal to 1/6 $\rho \cdot D_{ve}^3$. The detailed derivation of Eq. (8) was presented in Schneider et al. (2006). The ρ_e^I and ρ_e^{III} are demonstrated to have the inherent characteristics of decreasing with increasing particle size in a separate paper. Therefore, it will introduce systemic error when assessing the particle impacts on visibility, human health and climate from the physical quantities in ρ_e^I and ρ_e^{III}. In contrast, ρ_e^{II} is independent of particle size. Previously, ρ_e^{II} and the real part in the refractive index (n) can be retrieved from a fitting procedure that compares the measured light-scattering intensity of particles (R_{meas}) to the theoretical values ($R_{theory,test}$) calculated by a series of n and ρ_e^{II} values. Moffet and Prather (2005) successfully obtained ρ_e^{II} for spherical particles by single particle mass spectrometry. However, subject to the accuracy of Mie theory for the aspherical particles, dry NaCl and calcium-rich dust particles were failed to fit the $R_{theory,test}$ well to R_{meas} (Moffet et al., 2008). Similarly, Zhang et al. (2016a) failed to simultaneously retrieve ρ_e^{II} and n for $(NH_4)_2SO_4$ and $NaNO_3$ particles. To our best knowledge, there is no effective technique to achieve the measurement of ρ_e^{II} for aspherical particles. For reference, the symbol ρ_e in the following text refers to the definition of ρ_e^{II}.

The aim of the present work is to develop a method to obtain D_{ve} and ρ_e. The established system of an aerodynamic aerosol classifier (AAC)-single particle aerosol mass spectrometry (SPAMS) is capable of characterizing the D_a and D_{va} of particles,

which can be applied to theoretically derive D_{ve} and ρ_e. To verify the reliability of the AAC-SPAMS system, we apply it to measure the D_{ve} and ρ_e of the spherical particles of polystyrene latex (PSL). The results are in good agreement with the theoretical values. Finally, the AAC-SPAMS system is applied to measure the D_{ve} and ρ_e for $(NH_4)_2SO_4$ and $NaNO_3$ particles and for the chemically-resolved atmospheric particles.

2. Experimental section

2.1 Measurement system

Figure 1 shows a schematic diagram of the AAC-SPAMS system. The particles are first dried by a diffusion drying tube (TSI 9302, USA), classified by AAC (Cambustion Ltd., UK) based on the aerodynamic diameters D_a, and then transported into SPAMS in which the D_{va} and the mass spectra of individual particles are obtained. The working principle of the AAC is described in detail elsewhere (Tavakoli and Olfert, 2013). AAC consists of two coaxial cylinders that rotate at the same rotational speed. Polydisperse particles enter into the space between the cylinders (i.e., classification column) and experience a centrifugal force that causes them to move toward the outer cylinder. The particles to be classified can leave the classification column with the particle-free sheath flow and finally exit the AAC with the sample flow. Thus, the D_a values of classified particles can be derived from their relationship with their relaxation time (τ), as shown in Eq. (9):

$$\tau = \frac{C_C(D_a)\cdot\rho_0\cdot {D_a}^2}{18\mu} \quad (9)$$

where μ is the gas dynamic viscosity. Particles with large relaxation times impact and

adhere to the outer cylinder, while particles with small relaxation times exit the classifier with the exhaust flow. The exhaust flow from the AAC was about 0.3 lpm, and the Size Resolution Parameter (Rs) of the AAC was set as 40.

Detailed information about the operation of SPAMS (Hexin Analytical Instrument Co., Ltd., China) is described elsewhere (Li et al., 2011). Briefly, the particles are introduced into the vacuum system through a 0.1 mm critical orifice and are gradually collimated into a beam in the aerodynamic lens. Two continuous diode Nd:YAG laser beams (532 nm) are used to aerodynamically size the particles, which are subsequently desorbed/ionized by a pulsed laser (266 nm) that is triggered based on the velocity of a specific particle. The generated positive and negative ions are recorded with the corresponding particle size. The D_{va} of the particle is related to the transit time between the two laser beams (532 nm) in SPAMS, which can be obtained by using a calibration curve generated from the measured transit times of a PSL series with predefined sizes (nominal diameters).

2.2 Laboratory experiments

Dried spherical PSL (Nanosphere Size Standards, Duke Scientific Corp., Palo Alto) (ρ_p = 1.055 g/cm^3 and χ = 1.0) with D_{ve} values of 203.0 ± 5.0 nm, 310.0 ± 6.0 nm, 510.0 ± 5.0 nm, and 740.0 ± 6.0 nm were used in the AAC-SPAMS system, and the D_{ve} was verified by Scanning Mobility Particles Sizer (Model 3938, TSI Inc., USA). The PSL particles were first classified by AAC, and then their D_{va} values were obtained by SPAMS. ACC-SPAMS was also applied to the particles of $(NH_4)_2SO_4$ (ρ_p = 1.77 g/cm^3)

and $NaNO_3$ (ρ_p = 2.26 g/cm^3) with D_a values of 250.0 nm, 350.0 nm, 450.0 nm and 550.0 nm.

2.3 Ambient sampling

For field observations, the AAC-SPAMS system was placed in science and technology enterprise accelerator A2 Block, Guangzhou, China, to characterize the D_{ve}, ρ_e and chemical compositions of aerosol particles. The sampling inlet was hung 2.5 meters from the third floor (~12 m above ground level). Ambient aerosol particles were introduced into the AAC through a 5 m long conductive silicone tube with an inner diameter of 6 mm and a $PM_{2.5}$ cyclone inlet. The overall sampling flow was 3 lpm, and the residence time was approximately 5 seconds. Sampled particles were classified by the AAC as one of four D_a: 250.0 nm, 350.0 nm, 450.0 nm and 550.0 nm. The sampling time for the particles of each D_a was approximately 10 minutes. From July 6th to 8th, 2019, approximately 129,869 ionized particles were obtained from nine rounds of measurement. The sampling details are shown in Table S1. The number of ionized particles with the D_a of 250.0, 350.0, 450.0, and 550.0 nm is about 35,609, 38,374, 31,910, and 23,976, respectively. The sampled ~100,000 particles are first classified by using an adaptive resonance theory neural network (ART-2a) (Song et al., 1999) with a vigilance factor of 0.75, a learning rate of 0.05 and 20 iterations.

2.4 Theoretical derivation of D_{ve} and ρ_e from D_a and D_{va}

D_{ve} is the accurate physical quantity of the size of a particle. ρ_e is an alternative property for ρ_p, which is consistent with the property of ρ_p in terms of being independent

of particle size. These two properties cannot yet be measured for unknown particles by current techniques. In this study, the calculations of D_{ve} and ρ_e for unknown particles are theoretically derived from D_a and D_{va}. Combining Eqs. (2) and (3), we obtain the following Eq. (10):

$$C_c(D_a)\frac{{D_a}^2}{D_{va}} = D_{ve}C_c(D_{ve})\frac{\chi_v}{\chi_t} \quad (10)$$

Based on the approximation between χ_v and χ_t ($\chi_v \approx \chi_t = \chi_a$) (DeCarlo et al., 2004), Eq. (10) becomes Eq. (11):

$$C_c(D_a)\frac{{D_a}^2}{D_{va}} = D_{ve}C_c(D_{ve}) \quad (11)$$

The Cunningham Slip Correction Factor is calculated by Eq. (12):

$$C_c(D) = 1 + \frac{\lambda}{D}\left(A + B \cdot \exp\left(\frac{C \cdot D}{\lambda}\right)\right), \quad (12)$$

where λ is the mean free path of the gas molecules, and A, B and C are empirically determined constants specific to the analysis system. Substituting Eq. (12) into Eq. (11) obtains the Eq. (13).

$$\frac{{D_a}^2}{D_{va}} + \frac{D_a \cdot \lambda}{D_{va}}\left(A + B \cdot \exp\left(\frac{C \cdot D_a}{\lambda}\right)\right) = D_{ve} + \lambda\left(A + B \cdot \exp\left(\frac{C \cdot D_{ve}}{\lambda}\right)\right) \quad (13)$$

Thus, if the D_a and D_{va} of an unknown particle can be measured, its D_{ve} will be calculated according to Eq. (13). Finally, the ρ_e value of the particles is calculated by the D_{va} and D_{ve} values according to Eq. (14), which is obtained by combining Eq.(3) and Eq.(5):

$$\rho_e = \frac{\rho_p}{\chi_a} = \frac{D_{va}}{\rho_0 \cdot D_{ve}} \quad (14)$$

Thus, we can obtain both the D_{ve} and ρ_e values of unknown particles based on the D_a and D_{va} values. Because the AAC and SPAMS instruments have the ability to determine D_a and D_{va}, the AAC-SPAMS system, which is developed in this study, can be used to

obtain the D_{ve} and ρ_e values for unknown particles.

3. Results and discussion

3.1 Verification of the AAC-SPAMS system to obtain D_{ve} and ρ_e

The D_{va} distribution of PSL particles with predefined D_{ve} values after screening by the AAC is shown in Figure S1. We used Gaussian fitting to obtain the peak D_{va} for each size PSL with an R-squared fitting coefficient (R^2) over 0.98. Each fitting has a full width at half maximum (FWHM) of 6.6%, 4.4%, 2.3% and 2.2%, and the corresponding peaks are 215.8 nm, 319.0 nm, 532.1 nm and 803.5 nm, respectively. Substituting the D_a and D_{va} values of PSL into Eq. (11), the measured D_{ve} ($D_{ve,me}$) of PSL from AAC-SPAMS system is 203.6 nm, 309.7 nm, 511.6 nm and 737.2 nm, respectively (Figure 2a). Thus, the deviations between the theoretical D_{ve} ($D_{ve,th}$) and $D_{ve,me}$ values are 0.3%, -0.1%, 0.3% and -0.4%, respectively. On the other hand, the measured ρ_e ($\rho_{e,me}$) values of the particles are calculated from the D_{va} and $D_{ve,me}$ values with Eq. (14), and the $\rho_{e,me}$ values are 1.1 g/cm^3, 1.0 g/cm^3, 1.0 g/cm^3, and 1.1 g/cm^3 (Figure 2b). The deviations of $\rho_{e,me}$ are determined to be 4.3%, -5.2%, -5.2%, and 4.3%, respectively, by comparing to the theoretical ρ_e ($\rho_{e,th}$) that is equals to the ρ_p for the spherical particles (i.e. 1.055 g/cm^3 of PSL particles). That is, the deviations of $D_{ve,me}$ and $\rho_{e,me}$ characterized by the AAC-SPAMS system are within 1% and 6%, respectively. We therefore conclude that the AAC-SPAMS system is highly accurate for obtaining aerosol D_{ve} and ρ_e.

3.2 Application of the AAC-SPAMS system for obtaining D_{ve} and ρ_e of $(NH_4)_2SO_4$ and $NaNO_3$

Figure S2 shows the D_{va} distributions of $(NH_4)_2SO_4$ and $NaNO_3$ particles, which have D_a values of 250.0, 350.0, 450.0, and 550.0 nm, as screened by the AAC. The D_{va} peaks are obtained by Gaussian fitting, with R^2 values over 0.93 and FWHM values ranging from 7.6% to 10.6%. The $(NH_4)_2SO_4$ particles have D_{va} values of 300.0, 418.0, 551.1, and 695.1 nm (Figure S2), which correspond to particles possessing $D_{ve,me}$ values of 177.3, 254.4, 331.8, and 409.3 nm, respectively, according to Eq. (11). Substituting the values of D_{va} and $D_{ve,me}$ into Eq. (12), the $\rho_{e,me}$ values are 1.7, 1.6, 1.6, and 1.7 g/cm^3 (Figure 3a), respectively. Similarly, the selected $NaNO_3$ particles are determined to have D_{va} values of 321.0, 454.9, 599.8, and 755.3 nm (Figure S2), corresponding to $D_{ve,me}$ values of 150.1, 218.2, 287.0, and 355.9 nm, respectively. The $\rho_{e,me}$ values of the $NaNO_3$ particles are 2.2, 2.0, 2.0, and 2.1 g/cm^3 for the four particle sizes (Figure 3b), respectively. Figure 3 also shows that the $\rho_{e,me}$ values of the $NaNO_3$ and $(NH_4)_2SO_4$ particles at four size deviate from their average values with the maximum of 5.9 % and 4.8%, respectively, which are identical with the deviation phenomenon for the $\rho_{e,me}$ of PSL particles. These deviations may be derived from the calibration of particle Dva from the SPAMS. While the R-square of size calibration curve is 0.999, the curve of exponential function is found to slightly deviate from the data points measured by SPAMS. For example, size calibration function has the deviation of -4.4% and 3.1% from the data points of 310 and 740 nm, respectively.

Taking the systematic error into account, the slight difference of the $\rho_{e,me}$ values for

233 the four sizes suggests that the ρ_e of $(NH_4)_2SO_4$ and $NaNO_3$ particles is independent of
234 particle size from 250.0 nm to 550.0 nm. It is determined by the definition of effective
235 density used in this study, which keeps constant as long as the χ_a of the particles does
236 not change with particle size for pure compound. The average $\rho_{e,me}$ values of $(NH_4)_2SO_4$
237 and $NaNO_3$ particles are calculated to be 1.7 ± 0.1 and 2.1 ± 0.1 g/cm^3, respectively.
238 The average $\rho_{e,me}$ values are lower than that the ρ_p of $(NH_4)_2SO_4$ (1.77 g/cm^3) and
239 $NaNO_3$ (2.27 g/cm^3), which is caused that the $\rho_{e,me}$ is determined by both of ρ_p and χ_a.
240 According to Eq. (14), the χ_a of $(NH_4)_2SO_4$ and $NaNO_3$ particles with different D_a are
241 calculated to be 1.04, 1.11, 1.11, and 1.04 and to be 1.03, 1.14, 1.14, and 1.08,
242 respectively. Thus, the average χ_a values of the $(NH_4)_2SO_4$ and $NaNO_3$ particles are
243 determined to be 1.07 ± 0.04 and 1.10 ± 0.05, respectively, which can be used to
244 parameterize their morphology.

245 The average χ_a values of the $(NH_4)_2SO_4$ and $NaNO_3$ particles indicate that these
246 particles are aspherical. The asphericity of $(NH_4)_2SO_4$ determined by AAC-SPAMS
247 system is consistent with the previous studies reporting that the χ_a of $(NH_4)_2SO_4$ were
248 larger than the value of 1.03 (Zelenyuk et al., 2006;Beranek et al., 2012;Zhang et al.,
249 2016a). However, previous studies found that the $NaNO_3$ particles had different
250 morphology. Zhang et al. (2016a) observed that $NaNO_3$ had the χ_a of 1.09-1.13,
251 indicating its asphericity, while Hoffman et al. (2004) found that $NaNO_3$ particle had a
252 round droplet-like shape even at 15% RH, which was supported by the consistence
253 between the measured value of "anhydrous" droplet density and the calculated value of
254 "anhydrous" solution droplet (Zelenyuk et al., 2005). Eclectically, Tang and

Munkelwitz (1994) studied that most of the $NaNO_3$ particles crystallized between 20% and 30% RH but some persisted down to 10% RH to form solution droplets. Notably, the spherical $NaNO_3$ particles at low RH observed by Hoffman et al. (2004) were dried in the sticky carbon tape which might affect the phase transition of droplet-like $NaNO_3$ particles. In this study, most $NaNO_3$ particles were crystallized because the RH of the aerosol flow carrying the $NaNO_3$ particles was reduced to below 20% through the diffusion drying tube. Besides, the result that the crystallized $NaNO_3$ particles are aspherical is supported by their FWHM values of the D_{va} distributions which are consistent with that of aspherical $(NH_4)_2SO_4$ but wider than spherical PSL (Figures S1 and S2).

3.3 Application of the AAC-SPAMS system for measuring the chemically-resolved D_{ve} and ρ_e

SPAMS can obtain information on the chemical composition of individual particles, implying that the AAC-SPAMS system has the ability to simultaneously characterize D_{ve}, ρ_e and the chemical compositions of particles in real time. It is worth noting that the particles with the largest χ in the actual atmosphere should be freshly emitted soot, which χ is 2.5 (Peng et al., 2016). This largest χ fitly meets the upper limit for the approximation between the χ_t and χ_v (DeCarlo et al., 2004). Therefore, the AAC-SPAMS system can obtain the chemically-resolved D_{ve} and ρ_e values for unknown aerosol particles in the field observation.

As an example, we applied the AAC-SPAMS system to illustrate how the measured

277 D_a, D_{va}, and chemical composition of an individual particle can be used to calculate the
278 D_{ve} and ρ_e for unknown particles. The sampled ~100,000 particles are classified into
279 eight major particle types with distinct chemical patterns of K-rich, EC-S, K-Na, Amine,
280 EC-N-S, OC-N-S and OC-EC-N-S and Metal-rich, representing 97% of the detected
281 particle population. Details of the chemical composition and number fraction of the
282 eight types of particles are presented in the Figure S3 and Figure S4, respectively, which
283 are discussed in the Supporting Information.

284 We used Gaussian fitting to obtain the D_{va} peaks for each particle type with D_a values
285 of 250.0 nm, 350.0 nm, 450.0 nm, and 550.0 nm. Then, we calculated the D_{ve} values of
286 the atmospheric particles with Eq. (11). Table 1 presents the average D_{ve} values of the
287 eight particle types, for which the standard deviation is calculated based on nine
288 samples. The average D_{ve} at D_a values of 250.0 nm, 350.0 nm, 450.0 nm, and 550.0 nm
289 has the following wide ranges: from 188.5 nm to 200.8 nm, 271.9 nm to 295.7 nm,
290 342.5 nm to 428.9 nm, and 397.3 nm to 570.9 nm, respectively, which are caused by
291 the chemical composition differences. The result indicates that particles with
292 significantly different D_{ve} might possess the same D_a. Furthermore, the large standard
293 deviation of D_{ve}, such as 21.9 nm for K-Na at 250.0 nm, 32.3 nm for OC-EC-N-S at
294 350.0 nm, and 44.3 nm for OC-N-S at 450.0 nm, indicates that the D_{ve} of particles is
295 remarkably different even for particles with the same type and same D_a.

296 According to D_{ve} and D_{va}, we calculated the ρ_e of each particle type with Eq. (12).
297 Figure 4 shows the variations of the ρ_e with D_{ve} for nine particle samples. For pure
298 compounds, such as $(NH_4)_2SO_4$ and $NaNO_3$ particle, ρ_e theoretically does not change

with particle size. However, the sampled particles have experienced complex atmospheric processes. Therefore, ρ_e has a very wide distribution for each type of particle with a similar D_{ve}. Specifically, the ρ_e of K-Na increases with D_{ve}, while the ρ_e of OC-N-S and OC-EC-N-S decreases with D_{ve}, which may be influenced by the particle shape or the material density. Additionally, the average ρ_e of each type of particle is in the order from small to large: 1.2 ± 0.2 g/cm^3 for OC-EC-N-S, 1.3 ± 0.2 g/cm^3 for OC-N-S, 1.4 ± 0.1 g/cm^3 for K-rich, 1.4 g/cm^3 for Amine, 1.5 g/cm^3 for EC-N-S, 1.5 g/cm^3 for EC-S, 1.6 ± 0.1 g/cm^3 for K-Na and 1.6 ± 0.1 g/cm^3 for Metal-rich. It is reasonable to find that the average ρ_e of internally mixed particles distributes in the range of their material densities (ρ_m). For instance, mainly comprised of internally mixed sulfate and organics, the OC-EC-N-S, OC-N-S, K-rich, and Amine particles have the average ρ_e between that of sulfate with ρ_m of 1.77 g/cm^3 and organic aerosols with ρ_m of 1.2 g/cm^3 (Cross et al., 2007).

4. Conclusion

We first develop an AAC-SPAMS system to achieve the measurement of the D_{ve} and ρ_e of the particles through characterizing their D_a and D_{va}. The reliability of the AAC-SPAMS system is verified by accurately measuring the D_{ve} and ρ_e of PSL. Applying the AAC-SPAMS system to determine the D_{ve} and ρ_e of $(NH_4)_2SO_4$ and $NaNO_3$ particles shows that these particles are aspherical and their ρ_e are independent of particle size. Coupled with the ability of SPAMS to characterize the chemical composition of individual particles, we conducted a sample proof of the AAC-SPAMS equipment in

Guangzhou to first characterize the D_{ve}, ρ_e and chemical compositions of atmospheric particles, showing the potential application of this system in field observations. The approach achieves the measurement of chemically-resolved D_{ve} and ρ_e, and provides the possibility to determine their quantitative relationship with other particle properties, which would be benefit for further reduction of the uncertainty associated with the effects of particles on air quality, human health and radiative forcing.

Data availability. Data in this study is available at https://github.com/longer1217/All-figures-data.

Author contributions. The idea for the study was conceived by LP and GHZ. All experiments were performed by LP with the assistance of LL. LP wrote the paper which was reviewed by GHZ and XHB. All co-authors discussed the results and commented on the manuscript.

Competing interests. The authors declare they have no conflict of interest.

Acknowledgment

This work was supported by the National Nature Science Foundation of China (41775124 and 41877307), Natural Science Foundation of Guangdong Province (2019B151502022), and the Guangdong Foundation for the Program of Science and Technology Research (2019B121205006 and 2017B030314057). The authors also

gratefully acknowledge Cambustion Ltd., UK for providing the AAC and Hexin Analytical Instrument Co., Ltd., China for providing the SPAMS.

References

Beranek, J., Imre, D., and Zelenyuk, A.: Real-time shape-based particle separation and detailed in situ particle shape characterization, Anal. Chem., 84, 1459-1465, https://doi.org/10.1021/ac202235z, 2012.

Buseck, P. R., and Posfai, M.: Airborne minerals and related aerosol particles: effects on climate and the environment, P. Natl. Acad. Sci. USA, 96, 3372-3379, https://doi.org/10.1073/pnas.96.7.3372, 1999.

Cross, E. S., Slowik, J. G., Davidovits, P., Allan, J. D., Worsnop, D. R., Jayne, J. T., Lewis, D. K., Canagaratna, M., and Onasch, T. B.: Laboratory and ambient particle density determinations using light scattering in conjunction with aerosol mass spectrometry, Aerosol Sci. and Technol., 41, 343-359, https://doi.org/10.1080/02786820701199736, 2007.

DeCarlo, P. F., Slowik, J. G., Worsnop, D. R., Davidovits, P., and Jimenez, J. L.: Particle morphology and density characterization by combined mobility and aerodynamic diameter measurements. Part 1: Theory, Aerosol Sci. and Technol., 38, 1185-1205, https://doi.org/10.1080/027868290903907, 2004.

Guo, S., Hu, M., Zamora, M. L., Peng, J. F., Shang, D. J., Zheng, J., Du, Z. F., Wu, Z., Shao, M., Zeng, L. M., Molina, M. J., and Zhang, R. Y.: Elucidating severe urban haze formation in China, P. Natl. Acad. Sci. USA, 111, 17373-17378, 2014.

Hand, J. L., and Kreidenweis, S. M.: A new method for retrieving particle refractive index and effective density from aerosol size distribution data, Aerosol Sci. and Technol., 36, 1012-1026, https://doi.org/10.1080/02786820290092276, 2002.

Hoffman, R. C., Laskin, A., and Finlayson-Pitts, B. J.: Sodium nitrate particles: physical and chemical properties during hydration and dehydration, and implications for aged sea salt aerosols, J. Aerosol Sci., 35, 869-887, 2004.

Katrib, Y., Martin, S. T., Rudich, Y., Davidovits, P., Jayne, J. T., and Worsnop, D. R.: Density changes of aerosol particles as a result of chemical reaction, Atmos. Chem. Phys., 5, 275-291, https://doi.org/10.5194/acp-5-275-2005, 2005.

Li, L., Huang, Z. X., Dong, J. G., Li, M., Gao, W., Nian, H. Q., Fu, Z., Zhang, G. H., Bi, X. H., Cheng, P., and Zhou, Z.: Real time bipolar time-of-flight mass spectrometer for analyzing single aerosol particles, Int. J. Mass Spectrom., 303, 118-124, https://doi.org/10.1016/j.ijms.2011.01.017, 2011.

Liu, Y., and Daum, P. H.: Relationship of refractive index to mass density and self-consistency of mixing rules for multicomponent mixtures like ambient aerosols, J. Aerosol Sci., 39, 974-986, https://doi.org/10.1016/j.jaerosci.2008.06.006, 2008.

Liu, Z., Hu, B., Ji, D., Wang, Y., Wang, M., and Wang, Y.: Diurnal and seasonal variation of the PM2.5 apparent particle density in Beijing, China, Atmos. Environ., 120, 328-338, https://doi.org/10.1016/j.atmosenv.2015.09.005, 2015.

Moffet, R. C., and Prather, K. A.: Extending ATOFMS measurements to include refractive index and density, Anal. Chem. 77, 6535-6541, https://doi.org/10.1021/ac0503097, 2005.

Moffet, R. C., Qin, X., Rebotier, T., Furutani, H., and Prather, K. A.: Chemically segregated optical and microphysical properties of ambient aerosols measured in a single-particle mass spectrometer, J. Geophys. Res.-Atmos., 113, https://doi.org/10.1029/2007jd009393, 2008.

Peng, J. F., Hu, M., Guo, S., Du, Z. F., Zheng, J., Shang, D. J., Zamora, M., Zeng, L. M., Shao, M., Wu, Y. S., Zheng, J., Wang, Y., Glen, C., Collins, D., Molina, M., and Zhang, R. Y.: Markedly enhanced absorption and direct radiative forcing of black carbon under polluted urban environments, P. Natl. Acad. Sci. USA, 252, 2016.

Pitz, M., Cyrys, J., Karg, E., Wiedensohler, A., Wichmann, H. E., and Heinrich, J.: Variability of apparent particle density of an urban aerosol, Environ. Sci. & Technol., 37, 4336-4342, https://doi.org/10.1021/es034322p, 2003.

Poschl, U.: Atmospheric aerosols: Composition, transformation, climate and health effects, Angew. Chem. Int. Edit., 44, 7520-7540, https://doi.org/10.1002/anie.200501122, 2005.

Schneider, J., Weimer, S., Drewnick, F., Borrmann, S., Helas, G., Gwaze, P., Schmid, O., Andreae, M. O., and Kirchner, U.: Mass spectrometric analysis and aerodynamic properties of various types of combustion-related aerosol particles, Int. J. Mass Spectrom., 258, 37-49, https://doi.org/10.1016/j.ijms.2006.07.008, 2006.

Seinfeld, J. H., and Pandis, S. N.: From air pollution to climate change, 429-443, 1998.

Song, X. H., Hopke, P. K., Fergenson, D. P., and Prather, K. A.: Classification of single

409 particles analyzed by ATOFMS using an artificial neural network, ART-2A, Anal.
410 Chem., 71, 860-865, https://doi.org/10.1021/ac9809682, 1999.
411 Sumlin, B. J., Oxford, C. R., Seo, B., Pattison, R. R., Williams, B. J., and Chakrabarty,
412 R. K.: Density and homogeneous internal composition of primary brown carbon
413 Aerosol, Environ. Sci. & Technol., 52, 3982-3989,
414 https://doi.org/10.1021/acs.est.8b00093, 2018.
415 Tang, I. N., and Munkelwitz, H. R.: Water activities, densities, and refractive-indexes
416 of aqueous sulfates and sodium-nitrate droplets of atmospheric importance, J.
417 Geophys. Res.-Atmos., 99, 18801-18808, 1994.
418 Tang, I. N.: Thermodynamic and optical properties of mixed-salt aerosols of
419 atmospheric importance, J. Geophys. Res.-Atmos., 102, 1883-1893, 1997.
420 Tavakoli, F., and Olfert, J. S.: An instrument for the classification of aerosols by particle
421 relaxation time: theoretical models of the aerodynamic aerosol classifier, Aerosol
422 Sci. and Technol., 47, 916-926, https://doi.org/10.1080/02786826.2013.802761,
423 2013.
424 Yin, Z., Ye, X. N., Jiang, S. Q., Tao, Y., Shi, Y., Yang, X., and Chen, J. M.: Size-resolved
425 effective density of urban aerosols in Shanghai, Atmos. Environ., 100, 133-140,
426 https://doi.org/10.1016/j.atmosenv.2014.10.055, 2015.
427 Yon, J., Bescond, A., and Ouf, F. X.: A simple semi-empirical model for effective
428 density measurements of fractal aggregates, J. Aerosol Sci., 87, 28-37,
429 https://doi.org/10.1016/j.jaerosci.2015.05.003, 2015.
430 Zelenyuk, A., Cai, Y., Chieffo, L., and Imre, D.: High precision density measurements

of single particles: The density of metastable phases, Aerosol Sci. and Technol., 39, 972-986, https://doi.org/10.1080/02786820500380206, 2005.

Zelenyuk, A., Cai, Y., and Imre, D.: From agglomerates of spheres to irregularly shaped particles: Determination of dynamic shape factors from measurements of mobility and vacuum aerodynamic diameters, Aerosol Sci. and Technol., 40, 197-217, https://doi.org/10.1080/02786820500529406, 2006.

Zhang, G., Bi, X., Han, B., Qiu, N., Dai, S., Wang, X., Sheng, G., and Fu, J.: Measurement of aerosol effective density by single particle mass spectrometry, Science China Earth Sciences, 59, 320-327, https://doi.org/10.1007/s11430-015-5146-y, 2016a.

Zhao, G., Zhao, W., and Zhao, C.: Method to measure the size-resolved real part of aerosol refractive index using differential mobility analyzer in tandem with single-particle soot photometer, Atmos. Meas. Tech., 12, 3541-3550, https://doi.org/10.5194/amt-12-3541-2019, 2019.

446 **Table 1.** D_{ve} and its standard deviation for the eight particle types at D_a values of 250.0 nm, 350.0
447 nm, 450.0 nm, and 550.0 nm from nine round measurement.
448

D_a (nm)	K-rich	EC-S	K-Na	Amine
250.0	193.1 ± 8.2	192.2 ± 8.1	193.8 ± 21.9	190.6 ± 4.6
350.0	284.0 ± 28.4	280.8 ± 9.3	271.9 ± 18.0	284.8 ± 18.2
450.0	364.7 ± 21.1	357.8 ± 6.9	342.5 ± 7.3	367.9 ± 9.7
550.0	416.6 ± 28.3	439.5 ± 5.4	397.3 ± 29.7	442.5 ± 7.4
D_a (nm)	**EC-N-S**	**OC-N-S**	**OC-EC-N-S**	**Metal-rich**
250.0	188.5 ± 5.9	200.8 ± 17.9	195.4 ± 8.9	189.0 ± 6.7
350.0	281.3 ± 9.3	295.7 ± 29.8	294.0 ± 32.3	277.0 ± 9.1
450.0	358.0 ± 5.8	398.3 ± 44.3	428.9 ± 24.0	342.9 ± 10.0
550.0	453.2 ± 16.4	547.4 ± 14.7	570.9	407.4 ± 14.5

449

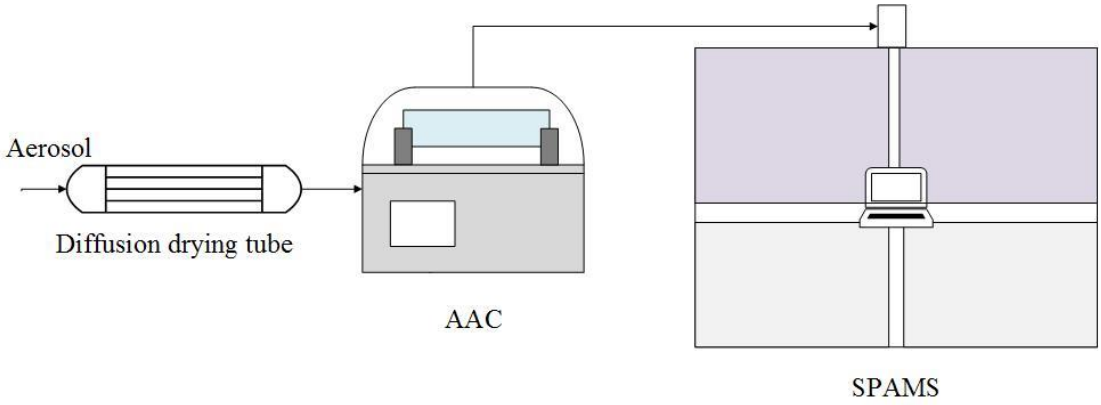

450

451 **Figure 1.** Schematic diagram of the AAC-SPAMS system (0.3 lpm). The diffusion drying tube is

452 filled with orange silica gel, which reduces the RH to 5-15%.

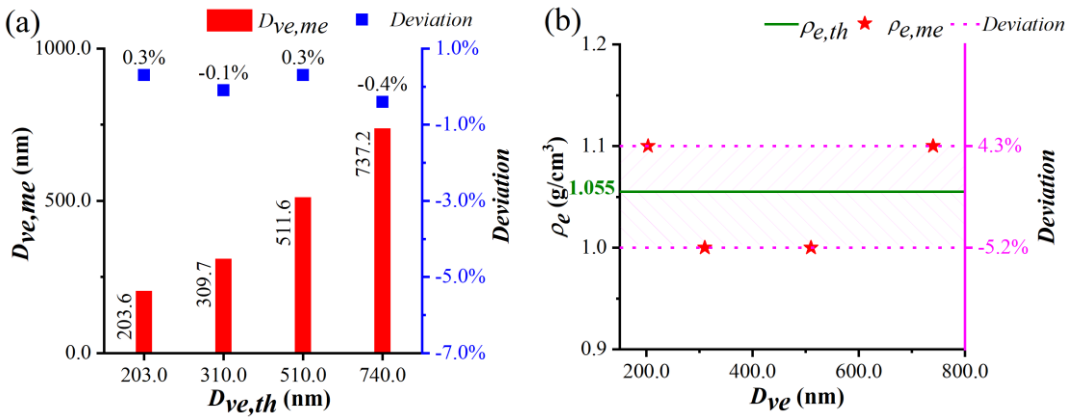

453

454

455 **Figure 2.** (a) Comparison between the measured D_{ve} ($D_{ve,me}$) and the theoretical D_{ve} ($D_{ve,th}$) of the

456 PSL particles. (b) Comparison between the measured ρ_e ($\rho_{e,me}$) and the theoretical ρ_e ($\rho_{e,th}$) of the

457 PSL particles.

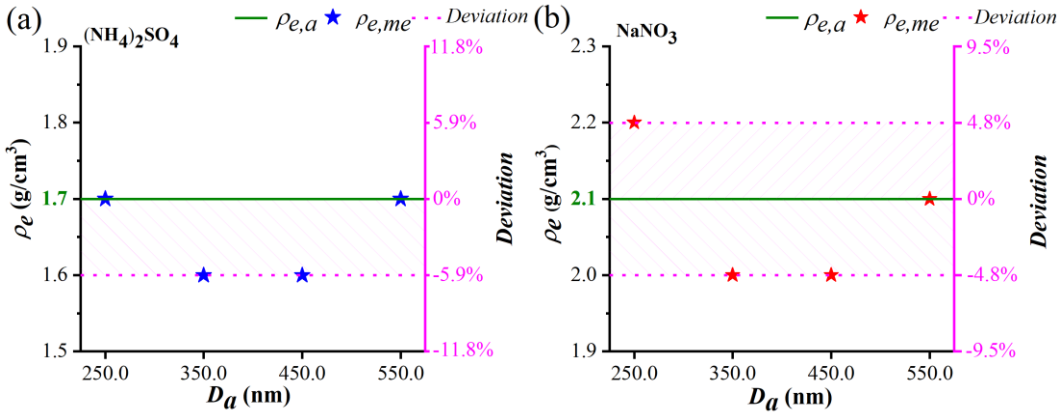

458

459

460 **Figure 3.** (a) Comparison between the measured ρ_e ($\rho_{e,me}$) and average ρ_e ($\rho_{e,a}$) values of the

461 $(NH_4)_2SO_4$ particles. (b) Comparison between the measured ρ_e ($\rho_{e,me}$) and average ρ_e ($\rho_{e,a}$) values of

462 the $NaNO_3$ particles.

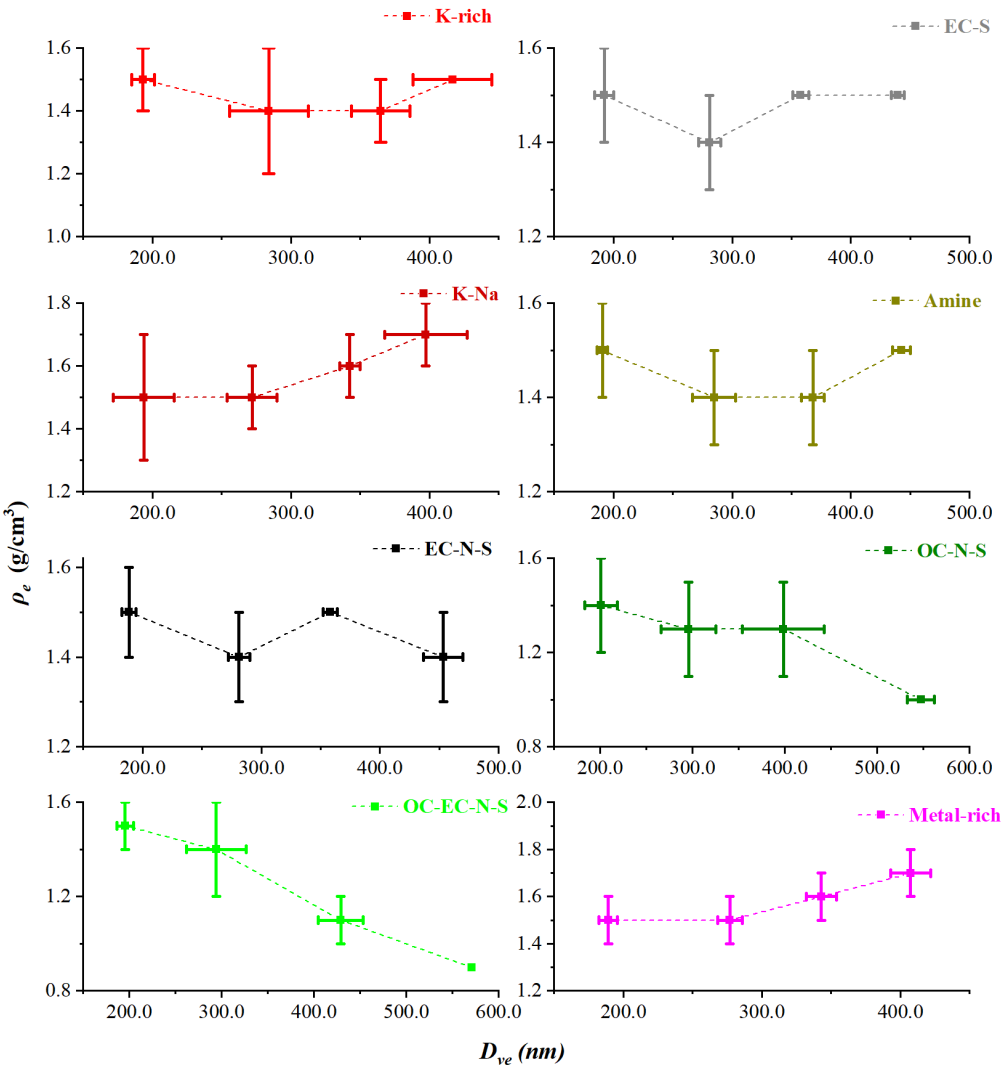

Figure 4. Variation in ρ_e of the eight particle types with D_{ve}. The solid lines represent the rang of the ρ_e and D_{ve} measured from nine rounds, and the data points stand for the average values.